ISBN: 978-3-95450-236-3 ISSN: 2673-5350 doi:10.18429/JACoW-IBIC2023-WEP001

NON-INVASIVE PROFILERS FOR THE COLD PART OF ESS ACCELERATOR

J. Marroncle, P. Abbon, F. Belloni, F. Bénédetti*, B. Bolzon, N. Chauvin, D. Chirpaz-Cerbat, M. Combet, M. Desmons, Y. Gauthier, T. Hamelin, C. Lahonde, P. Legou, O. Leseigneur, Y. Mariette, JP Mols, V. Nadot, M. Oublaid, G. Perreu, F. Popieul, B. Pottin, Y. Sauce, L. Scola, F. Senée, J. Schwindling, G. Tauzin, O. Tuske, S. Tzvetkov, CEA-Saclay, Gif-sur-Yvette, France
I. Dolenc Kittelmann, A. Gevorgyan, H. Kocevar, R. Tarkeshian, C. Thomas, ESS Lund, Sweden

Abstract

Several Non-invasive Profile Monitors are being installed along the accelerator to support the commissioning, tuning and operation of the powerful proton based ESS linear accelerator. In the low energy parts of the ESS linac (3.6 MeV to 90 MeV), the residual gas pressure is high enough to measure the transverse beam profile by using fluorescence induced by the beam on the gas molecules. However, in the ESS linac sections above 90 MeV, protons are accelerated by superconductive cavities working at cryogenic temperatures and high vacuum. Therefore, the signal based on the fluorescence process is too weak, while ionization can counteract this drawback.

We have provided five IPM (Ionization Profile Monitors) pairs for energies ranging from 100 to 600 MeV. The design of such monitors is challenging due to weak signal (as a result of high proton energy and low pressure $<10^{-9}$ mbar), tight space constraints inside the vacuum chamber, space charge effect, ISO-5 cleanliness requirement, and electrode polarization at ±15 kV.

This publication will detail the development we followed to fulfil the ESS requirements.

INTRODUCTION

The European Spallation Source (ESS) [1], presently under construction at Lund (Sweden), will consist of a 537 m long linear proton accelerator delivering a 2 GeV proton beam with a 5 MW power to a tungsten target, equipped with a highly optimized neutron moderator capable of providing a bi-spectral (thermal and cold) neutron beam to 42 beam ports, 22 of which are followed by a flight path leading to faraway measuring stations.

A perfect knowledge of the proton beam is critical for maximizing the number of protons on target and minimizing beam losses. Transverse beam profile monitors are therefore essential to support the tuning of the beam for good operation of the facility, both during its commissioning and in everyday operation.

Due to the high beam power, all beam profilers to be used at nominal operating conditions will be non-invasive type. In the frame of the in-kind contribution agreement signed with ESS, CEA has delivered to the European Spallation Source five Non-invasive Profile Monitors (NPMs) to be installed in the Cold Linac section: one in the Spoke section, 3 in the β-medium section, and one in the β-high section. These transverse beam profile monitors will cover proton energies ranging between 90 MeV and 600 MeV and are conceived to deliver one profile/pulse at a residual gas pressure of 10^{-9} mbar with an uncertainty on the beam width of less than 10% of its dimension (see Refs. [2] and [3] for a profiler detailed overview).

At such high proton energies and low residual gas pressure, the NPMs located on the superconductive beam line are based on the ionization of the residual gas. In the warm sections, transverse beam profiles are measured by using the fluorescence of the gas molecules induced by the beam.

ESS IPM DESCRIPTION

Two parts can be considered for describing an IPM (Fig. 1): the inner, situated inside the vacuum chamber, and the outer part. The beam traverses the cage approximately at its center.

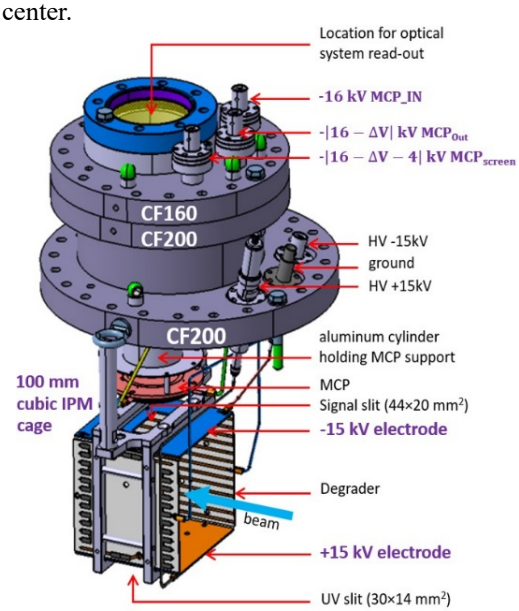

Figure 1: An ESS IPM.

Then, the ions and electrons, by-products of beam-residual gas interactions, drift under the influence of the electric field applied between both electrodes through a slit for ions before collection onto an MCP (Micro-Channel Plate). The MCP is equipped with a phosphorescent screen, allowing electric signal conversion to an optical one. To enhance the electric field uniformity, degraders positioned perpendicular to the electrodes are designed.

* Presently at LIPAc Rokkasho

ISBN: 978-3-95450-236-3 ISSN: 2673-5350 doi:10.18429/JACoW-IBIC2023-WEP001

On the outer part, the read-out is done with an optical system consisting of a lens and a CMOS camera. The HV connectors are used for the MCP and the cage polarization, linked with copper wires (1 mm). The control of the camera daq and the HV system is fully implemented in EPICS.

FEASIBILITY STUDY

When the project was initiated in mid-2016, several challenges were encountered that necessitated preliminary studies to assess the feasibility of such IPMs. These challenges can be summarized as follows:

- Ionization signal strength.
- Limited space inside the vacuum chamber.
- The space charge effect.
- Background particles that may hide or distort the profile, but were not inquired.
- ISO-5 cleanliness.

The following sections will be devoted to these topics.

Ionization Signal Strength

The nominal beam conditions for IPMs are low pressure, likely below 10^{-9} mbar, with a residual gas composition of H_2 (79%), CO (10%), CO_2 (10%) and N_2 (1% in mass), 62.5 mA beam intensity, and a beam width $\sigma_{X,Y}$ = 2 mm. During beam commissioning, the intensity may decrease to 1 mA, which will require an excess of read-out sensitivity.

Bethe's relation ([4] original) gives the mean energy losses by a charged particle per unit of media length; thus, knowing the average energy for producing ion/e pairs, we deduced their numbers in Table 1.

Table 1: e/ion Pairs Produced at Various Beam Energies

E (MeV)	97	280	628
e/ion (pairs/cm)	$1.0\ 10^5$	$4.9\ 10^4$	$3.4\ 10^4$

The electrode slit allowing the ions to pass toward the MCP is 2 cm large.

IPM Vacuum Chamber

The vacuum chamber, hosting a pair of Wire Scanners and a pair of IPMs, appears quite crowded, as illustrated in Fig. 2. The CF200 flanges (yellow) highlight their overlap. To address this issue, an adjustment is made by shifting the center of the IPM-X cage by 36 mm relative to the flange, enabling its insertion into the chamber.

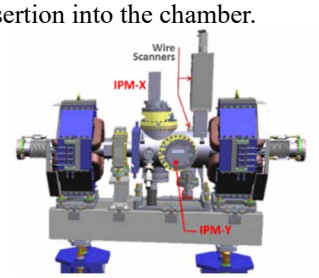

Figure 2: The Linear Warm Unit (LWU) comprises a vacuum chamber that includes 2 IPMs and 2 Wire Scanners.

In such a constrained space, two 100 mm cubic IPM cages, along with conductive discs, are securely attached to the chamber, perpendicular to the beam direction, and located 33 mm upstream and downstream from both IPM edges. The diameter of the hole in each disc is 100 mm, similar to that of the beam pipe. The purpose of these components is to ensure and improve the uniformity of the electric field inside the cage by grounding them as much as possible. In Fig. 3, a simulation conducted using COMSOL software [5] shows the original Gaussian profile achieved by a perfect field (green) and the reconstructed profile obtained by tracking (blue) ions into a realistic electric field taking into account the discs, which are in good agreement.

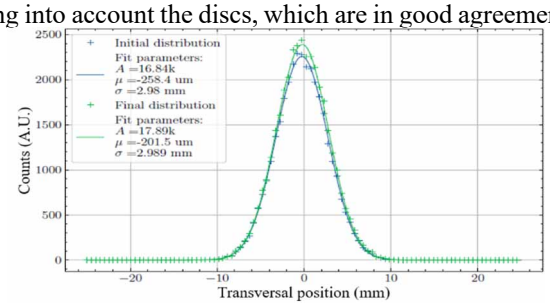

Figure 3: Gaussian profiles reconstructed by tracking for the original (green) and for the realistic profile (blue).

Space Charge Effect

One of the ESS requirements is to measure the beam width with a maximum total error in the RMS beam extension of less than ±10%. This becomes difficult to achieve in ESS conditions due to the space charge effect on the beam profile measurement.

The effects of space charge are twofold: they affect the charged particle beam and any other charge in its proximity. Our focus is on the later.

A charge generated at rest between two parallel plates kept at different voltages drifts towards the electrodes travelling parallel to the electric field lines. In an ideal case of a perfectly uniform electric field, the point where the charge meets the electrode will simply be the projection of its initial position on the electrode. In IPMs, charges are created via gas ionization, and the beam profile is reconstructed this way. However, the presence of a charged particle beam, necessary to create ionization charges, induces an electromagnetic field that modifies the trajectories of the electrons and the ionized gas molecules and thus introduces a shift between the point where they should have ideally met the electrode and the point where they reach it. The measured beam profile, therefore, will differ from the real one by an amount that depends on the beam intensity, the beam size, the beam energy, and the strength of the electric field applied between the electrodes.

Therefore, a simulation code was developed at CEA Saclay [6]. The momenta distributions for electrons are calculated using Garfield++ [7] while for ions the assumption $\overrightarrow{p_{ion}} = -\overrightarrow{p_e}$ was applied.

Calculations presented in Fig. 4 are performed for both ionization by-products, electrons and ions, versus the injected beam size into an IPM with a 300 kV/m electric field.

We observe that at ESS, the precision is consistently exceeds the required level for electrons. For ions, even at 90 MeV and a beam size larger than 2 mm, $|\Delta_X|$ is below

ISBN: 978-3-95450-236-3 ISSN: 2673-5350 doi:10.18429/JACoW-IBIC2023-WEP001

5%. The influence of the beam pulse diminish at higher energies due to pulse particle velocities, which reduce their impact on the scattered particles. As a result, IPMs must meet the requirements for beam width measurement, which can be achieved by establishing a high electric field inside their cages, around 300 kV/m.

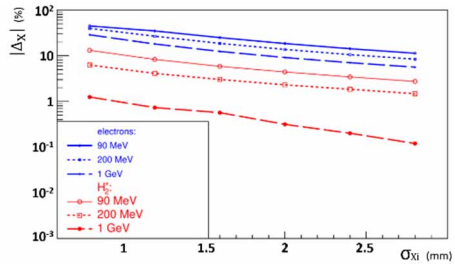

Figure 4: Space charge effect on the measured profiles for electrons and H_2^+ ions versus injected beam size. The IPM electric field is 300 kV/m.

ISO-5 Cleanliness

Due to their proximity to the superconductive cavities, IPMs must be delivered at ESS with a high cleanliness level, namely ISO-5, to prevent dust contamination and limit field emission. This implies that their designs must integrate compliant materials and that the test bench must be installed inside a laminar air flux.

The deployed logistics are pretty heavy, as listed below:

- Washing and rinsing all components in an ultrasonic bath,
- Transporting them in a basin filled with dezionized water to an ISO-7 clean room to prevent dust deposition,
- Moving them into an ISO-5 room for drying. Once completed, the integration of an IPM pair can start. An ionization gun with pure nitrogen gas is used for detaching particles, and a particle counter is used to check the ISO-5 level. All elements were mounted except the MCP and their copper wire connections.
- Finally, both IPMs are inserted into their vacuum chambers and wrapped inside a double ISO-5 plastic bag.
- The 5 IPM pairs follow these procedures and are stored in a laboratory.
- Then, we started integrating one pair, followed by another, into the test bench inside a laminar air flux. Baking is necessary as soon as the MCP comes in contact with air. Several mounting, dismounting are necessary due to the narrow space devoted to IPMs, which are finally characterized.
- The IPM survey and insertion inside its vacuum chamber are performed in a laboratory to pump and ensure that the IPM can travel in a static vacuum.

Feasibility Conclusion

The identified challenges have been largely addressed, with only a few minor difficulties encountered. Following a thorough review, the design of prototypes started. In the subsequent sections, we present some results from the prototype testing using a 3 MeV proton beam at the IPHI accelerator located at CEA Saclay [8].

PROTOTYPE TESTS AT IPHI

Three types of IPM were designed: A) equipped with an MCP featuring a phosphorescent screen and an optical read-out (lens + CMOS); B) incorporating conductive strips engraved on an electrode with the read-out of the strip current; C) similar to B) but with the addition of a simple MCP set before the strip plate for amplifying the strip current.

The optimal MCP can be polarized in asymmetric mode, one grounded electrode and the other at the HV, or in symmetric mode, meaning electrode polarization at ±HV.

We also have solid scintillators for comparison. All these instruments were inserted into a large vacuum chamber, moved in 2018 to IPHI, delivering a proton beam at 3 MeV working between 0.7 mA to 40 mA in pulse mode (0.1 to 1 ms) at 1 Hz during our tests.

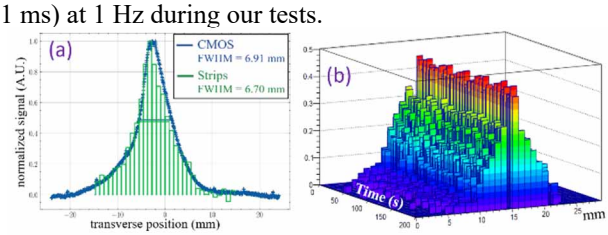

Figure 5: Strip and CMOS profile comparison (a). Profile measured for every pulse with MCP amplifying current (b).

First conclusion: A more sensitive integration-electronic for sampling the strip current is needed. However, it works very well when the physical signal is amplified by a simple MCP, which is quite similar to the optical read-out profile, as shown in Fig. 5a.

Second conclusion: We have opted for the optical read-out system due to the potential issues arising from the connections inside the beam pipe associated with the strip option, which may be challenging to resolve. Additionally, the strip option necessitates the use of an MCP, introducing a second fragile element in the system.

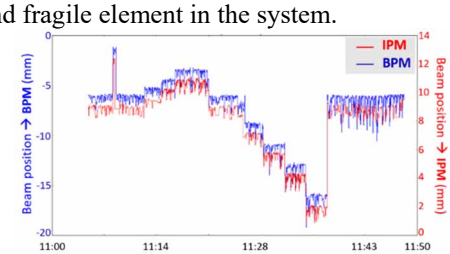

Figure 6: Correlations between IPM and BPM.

Figure 5b shows the ability to measure the beam profile for every pulse using the IPM equipped with an MCP amplifier of the strip currents, similar to the optical IPM.

During the experiment, we noticed a “slow” shift of the beam profile, which came back swiftly to the same position after a while. Initially, some electronic charge loading and discharging were suspected. However, a strong correlation between IPM and beam position monitor (BPM) favoured an objective observation of beam position shift, as shown

ISBN: 978-3-95450-236-3 ISSN: 2673-5350 doi:10.18429/JACoW-IBIC2023-WEP001

in Fig. 6, with a small disagreement due to monitor calibrations.

A few other interesting results were obtained, such as:

- Beam width convergence, refers to the electric field threshold above which the beam width stays constant. The optical IPM achieved this at around 100 kV/m for a 10 mA beam intensity and 125 kV/m at 30 mA.
- The beam size variation was studied with an IPM when the perpendicular electric field of a second IPM was varied from 0 to 200 kV/m. The beam size increases by less than 75 µm. The same study, but for the beam position, shows a displacement of around 0.4 mm. For both studies, there was no correction of the beam deviation induced by the upstream IPM in the downstream one.
- The uniformity of the electric field was assessed in the center of the IPM by sweeping the beam inside the cage. Results are consistent with expectations. To illustrate, a thin conductive 100 µm weft mesh was placed above the slit to enhance the electric field. In Fig. 7, a CMOS image captures the fine grid weft, confirming the uniformity of the electric field.

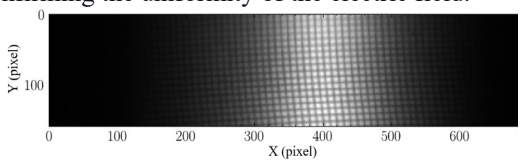

Figure 7: Beam signal observed through the mesh.

The main conclusion of this test is the extrapolation of IPHI data to ESS experimental conditions. For doing this, we requested a stable low beam intensity of 0.7 mA by 50 µs pulses (1 Hz) with 4 10^{-8} mbar residual gas pressure. Taking all these conditions, the cross-section ratios and the gas composition, results in a signal higher at 97 MeV and at 1.6 GeV, but 0.9 times lower at 2 GeV compared to ESS. Thus, we decided to modify the optical IPM mainly by:

- Taking a double MCP with a P43 phosphorescent screen for increasing the gain and their lifetimes
- Polarizing the IPM in symmetrical mode, -15 kV and +15 kV which improves the electric field uniformity
- Modifying the mechanics to give easier access to the MCP (weakest element) and having the same pieces for X and Y thanks to a rotating trick.

The final IPM versions take into account these remarks.

IPM INTEGRATION AND TEST

The first phase of ISO-5 integration is time consuming, mainly due to achieving ISO-5 standards with Macor materials. During the second phase of integration finalization and HV tests, several issues arose, with the most notable ones including:

- Correctly crawling the connection cables into the narrow chamber to set them at reasonable distances from grounded items. Several short circuits were induced, implying the need to break the vacuum, fix wire position, and bake necessitating at least one week.
- For minimizing matter, MCPs are screwed on 3 pillars, which must be tightened by fingers, but this was not mentioned by the provider. Therefore, a few of them were broken, particularly after baking. Finally, the solution was found by releasing slacks at screw level (Fig. 8). A small spring was added on each screw (Fig. 8(b)) to give longitudinal slack, while screws were filed on the top thread part for releasing transversal slack (Fig. 8(c)).

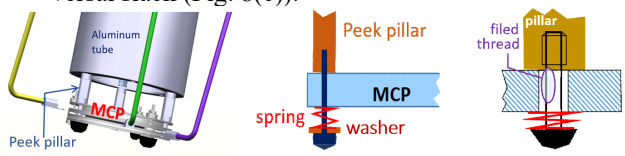

Figure 8: MCP fixed on 3 pillars (a), spring for longitudinal slack (b), filed thread for transverse slack (c).

To check the MCP gain, we used a UV lamp, which is fixed on the opposite side of the IPM vacuum chamber. UV photons have to cross a quartz viewport, and a small slit centred in the +15 kV electrode, the second slit (-15 kV) before reaching the MCP. Such a result is shown in Fig. 9.

Our acceptance criteria was IPM is validated when it is able to sustain ±15 kV with a $\Delta MCP_{In\text{-}Out} \gtrsim 1.3$ kV for more than 24 hours. This means that MCP is polarized at -16 kV for In, -14.7 kV for Out, and -10.7 kV for the Screen.

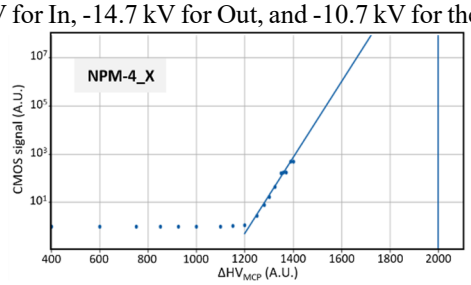

Figure 9: MCP gain measured with a UV lamp.

To complete the IPM processing, it is surveyed with a 3D Faro arm before being inserted into a vacuum chamber. Then, it is pumped once again at around 10^{-7} mbar, ready to be sent to ESS Lund under static vacuum. Finally, the 10 IPMs were delivered in pairs, the latest in August 2023.

CONCLUSION

The processes involved in the design, assembly, testing, and validation of the 10 IPMs for the cold section of the ESS accelerator have been succinctly described.

The challenge of operating the IPMs in a symmetric polarization mode at ±15 kV was encountered. The read-outs of the IPMs are facilitated by a CMOS camera utilizing an MCP equipped with a phosphorescent screen. One of the most demanding requirements was the achievement of ISO-5 cleanliness quality, which necessitated a significant logistical effort complicated by the limited space within the vacuum chamber.

All IPMs have been delivered to ESS Lund and are currently undergoing testing or installation stages.

The authors wanted to thank Stéphane Berry, Pierre Bosland and Catherine Madec, who kindly taught, advised and helped us achieve ISO-5.

ISBN: 978-3-95450-236-3 ISSN: 2673-5350 doi:10.18429/JACoW-IBIC2023-WEP001

REFERENCES

[1] R. Garoby *et al.,* "The European Spallation Source Design", *Phys. Scr.*, vol. 93, no. 12, p. 014001, 2018. doi:10.1088/1402-4896/aa9bff

[2] F. Bénédetti, "Design of non-invasive profile monitors for the ESS proton beam", Ph.D. thesis, Phys. IRFU/DEDIP, CEA Paris Saclay, France, 2019. [IRFU-19-22-T]

[3] F. Bénédetti *et al.,* "Design and Development of Ionization Profile Monitors for the Cryogenic sections of the ESS Linac", in *Proc. ANIMA 2019*, Portoroz, Slovenia, June 2019. doi:10.1051/epjconf/202022501009

[4] H. Bethe, "Zur Theorie des Durchgangs scheneller Korpuskularstrahlen durch Materie", in Annalen der Physik, vol. 397, no. 3, pp. 325-400, 1930. doi:10.1103/PhysRevLett.114.050511

[5] COMSOL, Inc, COMSOL Multiphysics 5.3a Reference Manuel, 2019. https://www.comsol.com/

[6] F. Belloni *et al.*, "Space Charge Effects Studies for the ESS Cold Linac Beam Profiler", in *Proc. IBIC'18*, Shanghai, China, Sep. 2018, pp. 371-374. doi:10.18429/JACoW-IBIC2018-WEOC04

[7] K. Baraka, S. Biagi, A. Folkestad, J. Renner, H. Schindler, N. Shiell, I. Smirnov, R. Veenhof, and K. Zenker, "Garfield++ simulation of tracking detectors", http://garfieldpp.web.cern.ch/garfieldpp

[8] R. Gobin *et al.,* "High Intensity Beam Production at CEA/Saclay For The IPHI Project", in Proc. ECRIS'16, Busan, Korea, Aug.-Sep. 2016, pp. 83-85. doi:10.18429/JACoW-ECRIS2016-WEPP01